A Novel Approach for Detection of Myocardial Infarction from ECG Signals of Multiple Electrodes

Rajesh Kumar Tripathy, Abhijit Bhattacharyya, and Ram Bilas Pachori

***Abstract*—Myocardial infarction (MI) is also called the heart attack, and it results in the death of heart muscle cells due to the lacking in the supply of oxygen and other nutrients. The early and accurate detection of MI using the 12-lead electrocardiogram (ECG) is helpful in the clinical standard for saving the lives of the patients suffering from this pathology. This paper proposes a novel approach for the detection of MI pathology using the multiresolution analysis of 12-lead ECG signals. The approach is based on the use of Fourier-Bessel series expansion based empirical wavelet transform (FBSE-EWT) for the time-scale decomposition of 12-lead ECG signals. For each lead ECG signal, nine subband signals are evaluated using FBSE-EWT. The statistical features such as the kurtosis, the skewness, and the entropy are evaluated from the subband signals of each ECG lead. The deep neural network (DNN) such as the deep layer least square support vector machine (DL-LSSVM) which is formulated using the hidden layers of sparse auto-encoders and the LSSVM is used for the detection of MI from the feature vector of 12-lead ECG. The experimental results demonstrate that the combination of FBSE-EWT based entropy features and DL-LSSVM has the mean accuracy, the mean sensitivity and the mean specificity values of 99.74%, 99.87%, and 99.60%, respectively for the detection of MI. The accuracy value of the proposed method is improved by more than 3% as compared to the wavelet-based features for the detection of MI.**

***Index Terms*—Myocardial Infarction, 12-lead ECG, FBSE-EWT, Clinical Information, DL-LSSVM.**

I. Introduction

MYOCARDIAL infarction (MI) is a cardiac pathology, and it arises due to the deprivation in the flow of the blood in the walls of the coronary arteries of the heart because of the deposition of thrombus and fibrin [1]. The major risk factors for MI are the formation of high blood cholesterol (the major reason for deposition of the thrombus in the artery walls), lack of exercise, higher consumption of alcohol, high blood pressure, stress, diabetes, and improper diet [2]. The progression of MI mainly happens in three major phases such as the primary phase which is termed as the myocardial ischemia (formation of atherosclerosis plaque due to the deposition of thrombus), the acute phase, and finally, the necrosis phase which arises due to lack of oxygen and other nutrients in heart muscle cells, resulting the death of heart muscle cells or heart attack [3]. In the clinical study, the patient with suspected MI symptoms immediately undergoes 12-lead electrocardiogram (ECG) test for the diagnosis, and for the localization of different types of MI, the pathological patterns in various ECG leads are also investigated [4]. Therefore, 12-lead ECG is one of the gold standard diagnostic modalities for accurate assessment and localization of MI pathology.

In recent years, various techniques have been applied for the automated detection of MI using 12-lead ECG signals [5] [6]. These techniques have evaluated features from ECG signal using various signal processing approaches and used different supervised learning algorithms for the MI detection. In [7]–[10], authors have used various time-domain morphological features from 12-lead ECG and classifiers such as K-nearest neighbor (KNN), support vector machine (SVM), artificial neural network (ANN), and neuro-fuzzy system for the detection and classification of MI. Some of the techniques have used heart-beat interval features, ST-segment features, and rough set based features for the detection of MI [11]–[13]. The multi-instance learning (MIL) based detection of MI pathology using 12-lead ECG has been reported in [14]. The authors have extracted ST-segment samples from each lead ECG and used polynomial regression for evaluating the coefficients. They have used the coefficients of ST-segments of 12-lead ECG as features for the detection of MI. The accurate detection of ECG on-set points along each lead is the prerequisite for the time-domain feature extraction approaches for MI detection. Moreover, the approaches based on the wavelet analysis of 12-lead ECG for the detection of MI have been reported in [15]–[18]. The shortcomings of wavelet-based approaches for the detection of MI are the requirement of the scaling and wavelet functions as priors for the time-scale decomposition of 12-lead ECG, and the selection of the number of decomposition levels.

The investigation of new features or bio-markers which can effectively capture the pathological variations in 12-lead ECG during MI and other heart pathological cases is an interesting research problem. Recently, the empirical wavelet transform (EWT) has been applied for the segmentation of heart sounds and the classification of murmurs from the phonocardiogram (PCG) signal [19]. This paper explores the Fourier-Bessel series expansion

Rajesh Kumar Tripathy, is with the Department of Electrical and Electronics Engineering, Birla Institute of Technology and Science (BITS) Pilani, Hyderabad Campus, India. e-mail: rajeshiitg13@gmail.com

Abhijit Bhattacharyya, is with the Department of Electronics and Communication Engineering, National Institute of Technology Andhra Pradesh, Tadepalligudem-534102, India. e-mail: abhijit9800@gmail.com

Ram Bilas Pachori is with Discipline of Electrical Engineering, Indian Institute of Technology Indore, Indore-453552, India. e-mail: pachori@iiti.ac.in

based EWT (FBSE-EWT) for time-scale analysis of 12-lead ECG, and the extraction of various features. It should be noted that in comparison to conventional EWT, the subband signals extracted using FBSE-EWT method match more firmly to actual narrow-band signal components [20]. Apart from this, due to the compact spectral representation of signals in the FBSE domain with better resolution, the FBSE-EWT method is very effective to estimate closely spaced frequency components in the analyzed signals. These facts were strongly presented in [20] with improved time-frequency representations of multicomponent synthetic signals, and real electroencephalogram (EEG) signal using the FBSE-EWT method. These salient characteristics inspired us to decompose the analyzed 12-lead ECG signals using the FBSE-EWT method, and thereby, extracted features from the subband signals. Recently, the deep learning techniques such as the convolutional neural network (CNN) and deep belief network (DBN) have been used for the detection of MI, and atrial fibrillation (AF) from ECG signals [21]–[23]. The multiple restricted Boltzmann machine (RBM) layers in DBN, and the repeated convolutional and pooling layers in CNN provides a better representation of ECG feature vector and, thus giving a higher performance for the detection of heart pathology. The sparse autoencoder has the flexibility to project the input feature vector to a higher dimension based on the increase in the number of hidden neurons with sparsity constraint [24]. The least square-support vector machine (LSSVM) classifier is very successful in detecting cardiac, and neural disorders from ECG and EEG signals [25], [26]. Therefore, a deep neural network (DNN) formulated by considering the multiple hidden layers of sparse autoencoder networks, and LSSVM classification layer can be used for the detection of MI pathology using 12-lead ECG features.

The major contributions of the paper are written as follows.

- The FBSE-EWT has been introduced for the time-scale analysis of normal and MI pathology based 12-lead ECG signals.
- The statistical features such as the skewness, kurtosis, and entropy are evaluated from the subband signals of each lead ECG.
- A novel DNN architecture which is based on sparse autoencoder, and LSSVM is proposed for the detection of MI.

The remaining sections of the paper are organized as follows. In Section II, the proposed method for the time-scale analysis of 12-lead ECG signals is described. The descriptions of the deep layer-LSSVM (DL-LSSVM) classifier for the detection of MI using 12-lead ECG features are given in Section III. In Section IV, the results and discussions are written. Finally, the conclusions of this paper are drawn in section V.

II. Method

In this section, the proposed approach for the detection of MI is presented. The approach mainly comprises of two sub-blocks such as, the diagnostic feature extraction from 12-lead ECG data matrix, and detection of MI using DNN. The diagnostic feature extraction process as shown in Fig. 1 consists of the 12-lead ECG data collection, filtering and segmentation of 12-lead ECG data matrix, FBSE-EWT based time-scale decomposition of 12-lead ECG matrix, and evaluation of various statistical features.

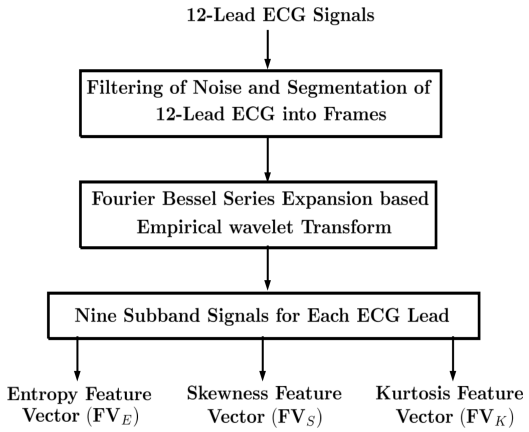

Fig. 1. Flow-chart for the evaluation of diagnostic features from 12-lead ECG using FBSE-EWT.

A. 12-lead ECG Data Collection

In this work, we have used the 12-lead ECG data matrix for healthy control (HC) and MI cases from Physikalisch Technische Bundesanstalt (PTB) diagnostic ECG database [27] [28]. This database comprises of 549 records of 15-lead ECG data, out of that the leads such as I, II, III, aVR, aVL, aVF, V1-V6 are 12-lead ECG signals, and the remaining three leads (V_x, V_y and V_z) are vectorcardiogram (VCG) signals. In this database, the sampling rate of each lead ECG signal is 1000 Hz, and the amplitude range is 16.384 mV with 16-bit resolution. In this study, we have taken 100, and 74 numbers of 12-lead ECG recordings from 100 MI and 52 HC subjects, and each 12-lead ECG recording has a duration of 24 hours.

B. Filtering and Segmentation of 12-lead ECG Data Matrix

The filtering process is applied to each 12-lead ECG data recording for HC and MI cases. The baseline wandering noise is filtered out using a Butterworth second order high-pass filter with the cutoff frequency as 0.5 Hz. The segmentation of the filtered 12-lead ECG data matrix is done using a rectangular window of size 4000×12. From each 24 hours recording of 12-lead ECG data, the non-overlapping frames are extracted. To capture all three types of correlations or similarities such as intra-beat, inter-beat and inter-lead in 12-lead ECG, we have used frame based segmentation technique [15]. The segmented 12-lead ECG frames are subjected to time-scale decomposition for the extraction of various features. Moreover, the high-frequency noise in each lead ECG signal is filtered out based on the selection of the corner frequencies using FBSE-EWT.

C. Time-Scale Decomposition of 12-lead ECG

In this study, the time-scale decomposition of 12-lead ECG signals is performed using FBSE-EWT. The EWT is a non-stationary signal decomposition method based on the idea of adaptive wavelet based filter bank structure [29]. These adaptive wavelet based filters in EWT are localized in the information location of the signal spectrum. The extracted signal components using EWT are compactly supported in the frequency domain with specific center frequencies. Recently in [20], authors have improved the existing EWT method with the inclusion of FBSE, which provides improved time-frequency representation with better estimation of signal components. In FBSE, the delaying (non-stationary) and aperiodic Bessel functions are used as the basis for the analysis and synthesis of signal [30]. The FBSE has been applied for the segregation of the monocomponent signals from the multicomponent non-stationary signal using discrete energy separation algorithim (DESA) and Wigner-Ville distribution (WVD) methods [30] [31]. The underlying concept of FBSE-EWT can be discussed using the following steps as [29]:

1) The FBSE method is employed for obtaining spectral representation of the analyzed signal in the frequency range $[0, \pi]$. The zero-order Bessel functions are used for the series expansion of the analyzed 12-lead ECG signal, $\mathbf{x}^m = [x^m(n)]_{n=1}^N$ with m as lead number ($m = 1, 2, ...M$, $M = 12$ is the total number of leads), n as number of samples with $n = 1, 2...N$, and it can be represented as [32]–[34],

$$x^m(n) = \sum_{k=1}^{K} P_k^m J_0\left(\frac{\varsigma_k n}{K}\right), \ n = 1, \ldots, N \quad (1)$$

where, P_k^m denotes the FBSE coefficients of $x^m(n)$ which can be represented as follows [32], [33]:

$$P_k^m = \frac{2}{K^2 (J_1(\varsigma_k))^2} \sum_{n=0}^{K-1} n x^m(n) J_0\left(\frac{\varsigma_k n}{K}\right) \quad (2)$$

where, $J_1(.)$ and $J_0(.)$ denote first and zero-order Bessel functions, respectively. The parameter ς_k with $k = 1, 2, \cdots K$ represents the positive roots of zero-order Bessel function ($J_0(.) = 0$). The relation between order k of FBSE coefficients and continuous time frequency F_k (in Hz) can be expressed as [32], [33],

$$\varsigma_k \approx \frac{2\pi F_k K}{F_s}, \text{ where } \varsigma_k \approx \varsigma_{k-1} + \pi \approx k\pi \quad (3)$$

where F_s denotes the sampling frequency.
The Equation (3) can also be represented as [33], [35],

$$k \approx \frac{2F_k K}{F_s} \quad (4)$$

Therefore, for covering the entire frequency range of the signal, the order k should be varied from 1 to K, which is same as the length of discrete time signal. Finally, the FBSE spectrum for m^{th} ECG lead can be obtained by plotting magnitude of the FBSE coefficients ($|P_k^m|$) versus frequencies (F_k). In [20], authors demonstrated that FBSE spectrum provides more compact spectral representation, and better frequency resolution as compared to the conventional discrete Fourier transform (DFT) based spectrum.

2) The scale-space based boundary detection method [36] is used to find the optimal boundary frequencies (φ_i), and to segregate FBSE spectrum into L number of contiguous segments. This requires the determination of $L + 1$ boundary frequencies. However, only $L - 1$ boundary frequencies are computed, as 0 and π are prefixed first and last boundary frequencies, respectively.
3) A set of band-pass filters are constructed in each segment using empirical scaling and wavelet functions. The wavelet based filters are built based on the construction idea of Littlewood-Paley and Meyer's wavelets [29], [37].

TABLE I
SCALING AND WAVELET FUNCTIONS USED IN EWT.

Functions	Mathematical expressions
Scaling [29]	$S_i(l) = \begin{cases} 1 & \text{if } \lvert l\rvert \le (1-\varepsilon)l_i. \\ \cos\left(\frac{\pi\mu(\varepsilon,l_i)}{2}\right) & \text{if } (1-\varepsilon)l_i \le \lvert l\rvert \le (1+\varepsilon)l_i. \\ 0 & \text{otherwise} \end{cases}$
Wavelet [29]	$W_i(l) = \begin{cases} 1 & \text{if } (1+\varepsilon)l_i \le \lvert l\rvert \le (1-\varepsilon)l_{i+1}. \\ \cos\left(\frac{\pi\mu(\varepsilon,l_{i+1})}{2}\right) & \text{if } (1-\varepsilon)l_{i+1} \le \lvert l\rvert \le (1+\varepsilon)l_{i+1}. \\ \sin\left(\frac{\pi\mu(\varepsilon,l_i)}{2}\right) & \text{if } (1-\varepsilon)l_i \le \lvert l\rvert \le (1+\varepsilon)l_i. \\ 0 & \text{otherwise.} \end{cases}$

In Table I, the mathematical expression of empirical scaling $S_i(l)$ and wavelet functions $W_i(l)$ are presented. The function $\mu(\varepsilon, l_i)$ in Table I is expressed as [29],

$$\mu(\varepsilon, l_i) = \gamma\left(\frac{(|l| - (1-\varepsilon)l_i)}{2\varepsilon l_i}\right) \quad (5)$$

where $\gamma(z)$ is an arbitrary function which is defined as follows [29]:

$$\gamma(y) = \begin{cases} 0, & \text{if } y \le 0. \\ \text{and } \gamma(y) + \gamma(1-y) = 1, & \forall y \in [0 \ \ 1] \\ 1, & \text{if } y \ge 1. \end{cases} \quad (6)$$

The condition of tight frame (in $L_2(R)$) of empirical scaling and wavelet functions is met by satisfying the following condition as [29],

$$\varepsilon < \min_i\left(\frac{l_{i+1} - l_i}{l_{i+1} + l_i}\right) \quad (7)$$

The detail coefficents $cD_j(s)$ ($j = 1, 2, ...J$, J is the total number of detail subbands) and approximation coefficients $cA_1(s)$ for m^{th} lead ECG have been computed by taking the inner product of the wavelets and scaling function with the ECG signal which can be expressed as [29],

$$cD_j^m(s) = \sum_{\tau=1}^{N} x^m(\tau)\overline{W_i(\tau - s)} \quad (8)$$

$$cA_1^m(s) = \sum_{\tau=1}^{N} x^m(\tau)\overline{S_1(\tau - s)} \tag{9}$$

Finally, the sub-band signals for j^{th} detail and approximation bands for m^{th} ECG lead are reconstructed as follows [29]:

$$x_{cD_j}^m(n) = \sum_{s=1}^{N_j} \mathbf{cD}_j^m(s) W_i(n-s) \tag{10}$$

$$x_{cA_1}^m(n) = \sum_{s=1}^{N_1} \mathbf{cA}_1^m(s) S_1(n-s) \tag{11}$$

where $x_{cD_j}^m(n)$ is the detail subband signal of j^{th} level, and $x_{cA_1}^m(n)$ denotes the approximation subband signal for m^{th} ECG lead. N_1 and N_j are the lengths of the wavelet coefficients vector for approximation, and j^{th} detail subbands.

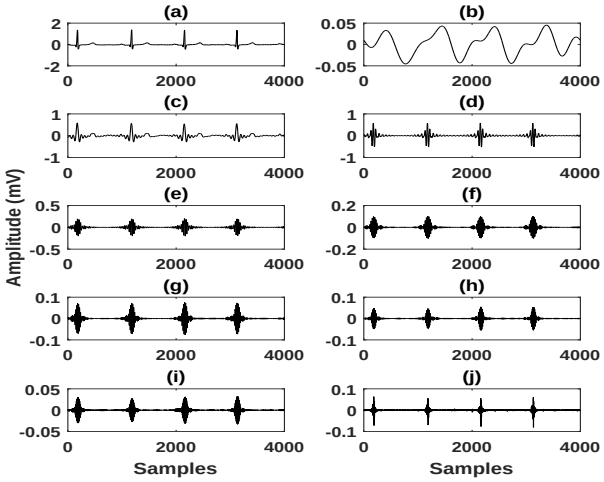

Fig. 2. (a) Lead V6 ECG signal for normal sinus rhythm or HC case. (b)-(j) Nine subband signals evaluated using FBSE-EWT based time-scale decomposition of lead V6 ECG.

The lead V6 ECG signals for HC and MI cases are depicted in Fig. 2(a), and Fig. 3 (a), respectively. It is evident from these two plots that, there are the variations in the T-wave morphology and inter-beat duration. The T-wave inversion is observed in MI cases as marked in red color in Fig. 3. These pathological changes can be captured using time-scale decomposition of lead V6 ECG signal using FBSE-EWT. The nine subband signals for HC and MI cases are shown in Fig. 2 (b)-(j), and Fig. 3 (b)-(j), respectively. It is also observed that the amplitude and the beat-to-beat variability for each subband signal are different in HC and MI cases. Henceforth, the features extracted from these subband signals can be used for the detection of MI. In this study, we have computed three different features such as the skewness, kurtosis, and entropy from each subband signal (total 9 subband signals for single lead ECG) for 12-lead ECG. The skewness (SK) feature for the t^{th} subband signal of m^{th} ECG lead is given by [38]

$$SK_t^m = \frac{E(x_t^m(n) - \mu_t)^3}{\sigma_t^3} \tag{12}$$

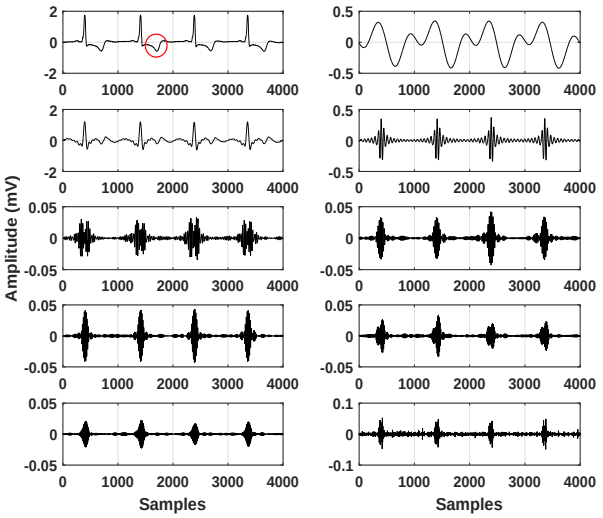

Fig. 3. (a) Lead V6 ECG signal for MI case (T-wave inversion is observed along each beat and it is marked in red color ellipse for the second ECG beat). (b)-(j) Nine subband signals evaluated using FBSE-EWT based time-scale decomposition of lead V6 ECG.

Similarly, the kurtosis (KR) feature for the t^{th} subband signal of m^{th} ECG lead is evaluated as [38]

$$KR_t^m = \frac{E(x_t^m(n) - \mu_t)^4}{\sigma_t^4} \tag{13}$$

where μ_t and σ_t are termed as the mean and the standard deviation values for t^{th} subband signal, and E is the expectation operator. The variable 't' is either approximate subband signal or detail subband signal and, $t \in (x_{cA_1}^m(n), x_{cD_j}^m(n))$ with $j = 1, 2...J-1$. Where J is the total number of subband signals evaluated using FBSE-EWT of each lead ECG. Moreover, the entropy for the t^{th} subband signal of m^{th} ECG lead is defined by [39]

$$EN_t^m = -\sum_{d=1}^{D} P_t^m(d) log[P_t^m(d)] \tag{14}$$

where $P_t^m(d)$ is the probability of d^{th} bin for the t^{th} subband signal of m^{th} ECG lead. The probability is evaluated based on the normalization of the histogram of each subband signal and, $D = 10$ is the number of bins in the histogram of each subband signal. From literature, it has been found that the wavelet entropy features from both single lead ECG and VCG have higher performance for the detection of MI pathology [40] [39]. The wavelet entropy has been evaluated based on the probability of each subband, and hence, this measure can quantify the global information of the ECG signal [40]. However, in the present work, we are evaluating the entropy (as in Equation (14)) from the histogram of each subband signal. It is expected that the proposed local entropy measure can effectively capture the pathological patterns in each subband signal of all 12-lead ECG signals for the detection of MI. In this study, for a single 12-lead ECG frame, 108 number of skewness features, 108 number of kurtosis features, and 108 number of entropy features are evaluated. The entropy, the

skewness, and the kurtosis feature vectors are formulated and these feature vectors (FVs) are denoted as $\mathbf{FV}_E$, $\mathbf{FV}_S$ and $\mathbf{FV}_K$, respectively. The performance of each feature vector (FV) is evaluated using DNN for the detection of MI.

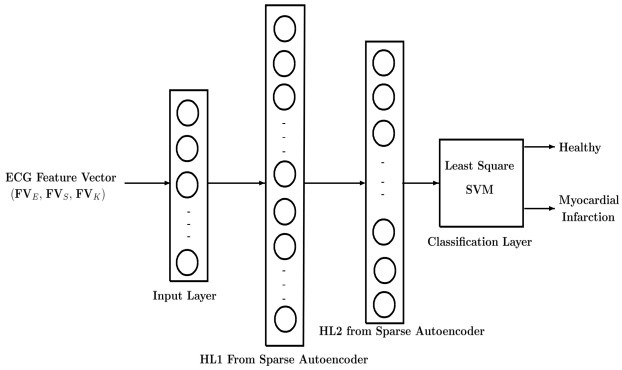

Fig. 4. Proposed DNN architecture for the detection of MI pathology.

III. DL-LSSVM for Detection of MI

In this section, the proposed DNN architecture which is termed as DL-LSSVM is described for the detection of MI. The DNN architecture is shown in Fig. 4, and it consists of the input layer, two hidden layers (hidden layer 1 (HL1) and hidden layer 2 (HL2)) and the LSSVM layer, respectively. The feature matrix contains the features for p number of 12-lead ECG instances and r number of features, and it is denoted as $\mathbf{Z} = [\mathbf{z}_i]$ with $i = 1, 2, ..., p$ and each $\mathbf{z}_i = [z_1^i, z_2^i, ..., z_r^i]$. Where $z_1^i, z_2^i, ..., z_r^i$ are the features for i^{th} 12-lead ECG instance. In this study, for each skewness FV ($\mathbf{FV}_S$), kurtosis FV ($\mathbf{FV}_K$) and entropy FV ($\mathbf{FV}_E$) case, the value of r is 108. Similarly, the output values for DL-LSSVM classifier for HC and MI classes are denoted as 0 and 1, respectively. The hidden layers of the DL-LSSVM network are evaluated from the encoder section of the deep sparse autoencoder network. For the sparse autoencoder, the weight matrix and bias at hidden layer are evaluated using the minimization of the cost function (C) as [24]

$$C(\mathbf{W}, \mathbf{b}) = \sum_{i=1}^{p} \left\| \tilde{\mathbf{z}}^i - \mathbf{z}^i \right\|_2^2 + \frac{\lambda}{2} \|\mathbf{W}\|_2^2 + \alpha \sum_{q=1}^{Q} KL(\frac{\rho}{\tilde{\rho}_q}) \quad (15)$$

The layer-wise pre-training approach is used for the evaluation of the activations of hidden layer neurons [41]. The first hidden layer weight matrix ($\mathbf{W1}$) is evaluated using the back-propagation algorithm (BPA) for the optimization problem of sparse autoencoder in Equation (15). Similarly, for the evaluation of the second hidden layer matrix ($\mathbf{W2}$), the first hidden layer (HL1) is considered as the input for the sparse autoencoder and BPA is again applied. The parameters such as ρ (sparsity parameter) and $\tilde{\rho}_q$ in the Kullback-Leibler (KL) divergence term are the desired frequency for the activation of hidden neurons and the average of the thresholded activation function for q^{th} hidden neuron, respectively [41]. After evaluating the weight matrices such as $\mathbf{W1}$ and $\mathbf{W2}$, the LSSVM model layer in the proposed DNN is used for the classification of HC and MI. The LSSVM classifier uses the least square cost function with equality constraint criteria for formulating the optimization problem [42], and this classifier has shown a better performance for the detection of pathologies using various biomedical signals [25] [26]. The performance of the DNN is evaluated using the objective measures such as accuracy, sensitivity, and specificity [15]. The selection of training and test 12-lead ECG frames for the DL-LSSVM is done using both hold-out (70% of 12-lead ECG frames as training and 30% frames as testing), and 5-fold cross-validation techniques [15].

IV. Results and Discussion

The proposed approach is evaluated using 12-lead ECG signals as outlined in Fig. 1 and Fig. 4, respectively. In this section, we have presented the statistical analysis of FBSE-EWT based 12-lead ECG features and the classification performance of DNN for MI detection. From the subband signals of HC and MI cases in Fig. 2, and Fig. 3, it is evident that the first two subband signals grossly capture the T-wave, and the low-frequency components of both QRS-complex and P-wave, respectively as the frequency ranges for P-wave, QRS-complex and T-wave are [5-30 Hz], [8-50 Hz] and [0.5 -10 Hz] [43]. Moreover, the mid-band and high-frequency components of the QRS complex are grossly segmented in the remaining seven subband signals. The variations in the morphologies of the clinical components of 12-lead ECG can be observed in the features from these subband signals. The intra-class distribution of selected kurtosis and entropy features from second and fifth subband signals of all ECG leads for HC and MI classes are depicted in Fig. 5 (a)-(d) and Fig. 5 (e)-(h), respectively. It is evident that the kurtosis feature from second subband signal of lead I ECG has a higher mean value for MI case as compared to HC case. For lead V1, the kurtosis feature from second subband signal has higher mean value for HC class. Similarly, significant differences in the mean values of kurtosis and entropy features from fifth and second subband signals for all ECG leads are also observed. Moreover, the entropy features from fifth subband signals of all ECG leads have higher mean values for MI case. Due to MI, the pathological symptom such as abnormal Q-wave in ECG leads and particularly, reciprocal variations in the morphologies for lead V1 and lead V2 ECG signals are seen [44]. The beat-to-beat variability in ECG is also different for MI and HC cases, and as a result, there are higher entropy values for high-frequency components of the ECG signals for all leads. The pathological signatures such as the T-wave inversion, ST-segment elevation are also observed in ECG signals for different leads [44]. These pathological symptoms may alter the shape of the probability density function (PDF) for low-frequency components of ECG signals. As the low-frequency components of 12-lead ECG signals are captured in the first two subband signals, so the kurtosis features have different mean values for HC

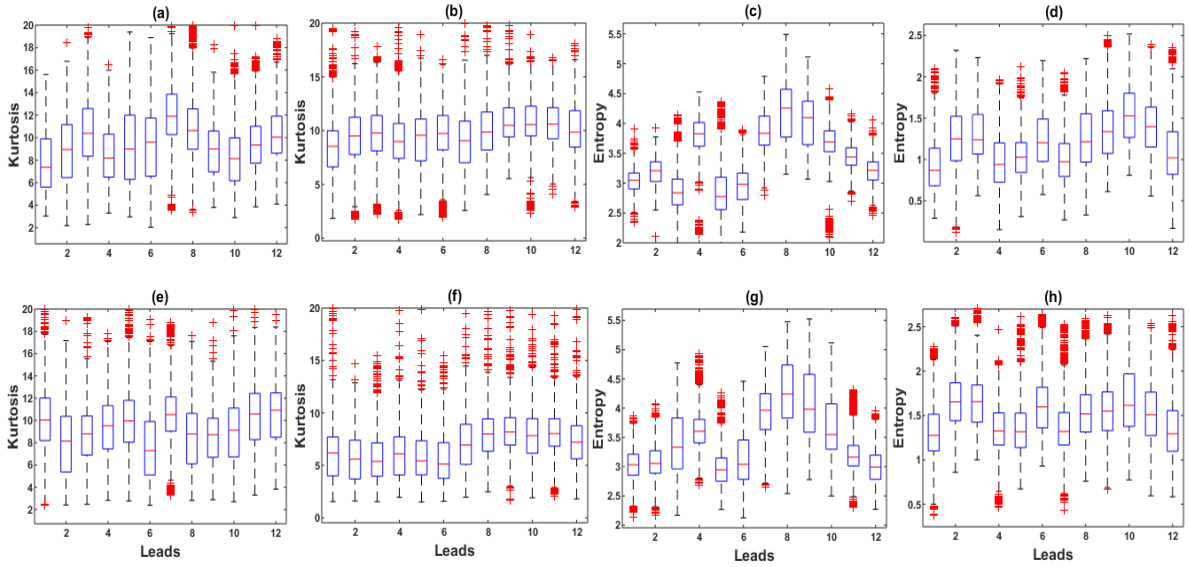

Fig. 5. (a) Boxplot for the kurtosis features from second subband signals of 12-lead ECG for HC class. (b) Boxplot for the kurtosis features from fifth subband signals of 12-lead ECG for HC class. (c) Boxplot for the entropy features from second subband signals of 12-lead ECG for HC class. (d) Boxplot for the entropy features from fifth subband signals of 12-lead ECG for HC class. (e) Boxplot for the kurtosis features from second subband signals of 12-lead ECG for MI class. (f) Boxplot for the kurtosis features from fifth subband signals of 12-lead ECG for MI class. (g) Boxplot for the entropy features from second subband signals of 12-lead ECG for MI class. (h) Boxplot for the entropy features from fifth subband signals of 12-lead ECG for MI class.

and MI classes. Moreover, the student t-test method is selected to evaluate the statistical significance of FBSE-EWT features [45]. From the t-test analysis, it is observed that out of 108 skewness features of 12-lead ECG, 26 and 33 features have p-values less than 0.001, and 0.05, respectively. Therefore, the skewness features of 12-lead ECG will have less performance for the detection of MI pathology. It is also evident from statistical analysis results that, 105, and 106 features have p-values less than 0.001, and 0.05 out of 108 kurtosis features of 12-lead ECG. Moreover, for entropy features of 12-lead ECG, we have 101 and 98 features with p-values lower than 0.05 and 0.01 out of 108 features. The lower p-values for more kurtosis and entropy features demonstrate that these features are statistically significant, and have the higher contribution to the classification of MI pathology and HC.

The performance of the DNN classifier is evaluated by considering skewness, kurtosis and entropy FVs of each ECG lead. For each lead ECG, the features from 9 subband signals are considered. The number of neurons in the first hidden layer and second hidden layer are 20 and 15, respectively. The performance of DNN classifier using the features from ECG signals of unipolar, bipolar and precordial leads are shown in Table II. It is evident that the performance of DNN classifier using entropy features is higher than the kurtosis and skewness features for each lead ECG. Moreover, it is also observed that the accuracy, sensitivity and specificity values of skewness features are less than 90% using DNN classifier. The skewness features fail to capture the pathological variation in the subband signals of each lead ECG and due to this reason these features have less performance for MI detection using DNN classifier. The anterior MI disease is detected based on the investigation of the pathological symptoms in ECG signals with lead numbers as V1, V2, V3, and V4, respectively [44]. Similarly, the medical practitioners examine the pathological changes in the lead sets such as (II, III, and aVF) and (I, aVL, V5 and V6) for the diagnosis of

TABLE II
PERFORMANCE OF DNN CLASSIFIER USING FVS FROM ECG SIGNALS OF UNIPOLAR AND BIPOLAR LIMB LEADS.

Leads	Measures	Skewness FV	Kurtosis FV	Entropy FV
I	Accuracy (%)	74.52 ± 2.21	95.32 ± 0.54	96.78 ± 0.54
	Sensitivity (%)	77.83 ± 2.80	95.73 ± 1.15	97.14 ± 0.81
	Specificity (%)	71.22 ± 2.85	94.92 ± 0.99	96.42 ± 0.98
II	Accuracy (%)	74.67 ± 1.85	95.18 ± 0.76	98.57 ± 0.52
	Sensitivity (%)	74.20 ± 1.63	94.51 ± 1.34	98.43 ± 0.75
	Specificity (%)	75.14 ± 2.82	95.86 ± 0.42	98.71 ± 0.52
III	Accuracy (%)	78.90 ± 0.91	94.12 ± 0.95	99.35 ± 0.14
	Sensitivity (%)	81.28 ± 2.44	95.64 ± 0.98	99.52 ± 0.19
	Specificity (%)	76.52 ± 1.20	92.60 ± 1.20	99.18 ± 0.23
aVR	Accuracy (%)	69.93 ± 1.87	94.54 ± 0.48	98.49 ± 0.56
	Sensitivity (%)	74.51 ± 2.42	93.07 ± 1.32	98.30 ± 0.68
	Specificity (%)	65.36 ± 1.46	96.01 ± 1.19	98.68 ± 0.90
aVL	Accuracy (%)	76.91 ± 1.04	94.85 ± 0.44	97.66 ± 0.93
	Sensitivity (%)	79.21 ± 2.22	94.57 ± 1.53	97.71 ± 0.32
	Specificity (%)	74.60 ± 2.41	95.14 ± 1.88	97.61 ± 1.96
aVF	Accuracy (%)	78.94 ± 1.69	96.17 ± 0.75	99.57 ± 0.11
	Sensitivity (%)	80.00 ± 1.46	95.42 ± 0.85	99.68 ± 0.24
	Specificity (%)	77.89 ± 2.87	96.92 ± 0.70	99.46 ± 0.17
V1	Accuracy (%)	64.51 ± 1.57	94.57 ± 0.34	99.27 ± 0.14
	Sensitivity (%)	68.58 ± 2.95	93.54 ± 0.80	99.46 ± 0.14
	Specificity (%)	60.43 ± 2.24	95.61 ± 1.12	99.09 ± 0.17
V2	Accuracy (%)	76.37 ± 1.73	94.95 ± 0.83	99.32 ± 0.37
	Sensitivity (%)	74.35 ± 1.79	97.21 ± 0.59	99.40 ± 0.33
	Specificity (%)	78.40 ± 2.94	92.69 ± 1.25	99.24 ± 0.66
V3	Accuracy (%)	82.21 ± 0.87	93.74 ± 0.65	99.21 ± 0.39
	Sensitivity (%)	85.36 ± 1.51	96.36 ± 0.88	98.99 ± 0.52
	Specificity (%)	79.05 ± 0.43	91.12 ± 1.54	99.43 ± 0.30
V4	Accuracy (%)	82.80 ± 0.66	94.59 ± 0.28	99.42 ± 0.18
	Sensitivity (%)	84.32 ± 1.25	96.70 ± 0.94	99.49 ± 0.33
	Specificity (%)	81.28 ± 1.55	92.47 ± 1.19	99.34 ± 0.23
V5	Accuracy (%)	78.88 ± 1.40	95.14 ± 0.40	98.63 ± 0.30
	Sensitivity (%)	79.90 ± 1.35	95.45 ± 1.17	98.77 ± 0.20
	Specificity (%)	77.86 ± 2.09	94.82 ± 1.58	98.49 ± 0.68
V6	Accuracy (%)	72.00 ± 1.43	94.73 ± 0.63	98.58 ± 0.41
	Sensitivity (%)	73.51 ± 0.49	94.32 ± 1.81	98.55 ± 0.58
	Specificity (%)	70.51 ± 2.41	95.14 ± 1.04	98.62 ± 0.51

TABLE III
PERFORMANCE OF DNN CLASSIFIER USING FVS FROM 12-LEAD ECG.

Measures	Skewness FV	Kurtosis FV	Entropy FV
Accuracy (%)	98.18 ± 0.24	99.23 ± 0.25	99.74 ± 0.21
Sensitivity (%)	98.21 ± 0.40	99.62 ± 0.17	99.87 ± 0.07
Specificity (%)	98.15 ± 0.20	98.84 ± 0.32	99.60 ± 0.40

inferior MI and lateral MI, respectively [15]. Moreover, the reciprocal changes in the ECG patterns for lead V1 and lead V2 are used for the diagnosis of posterior MI. The entropy and the kurtosis features effectively capture the pathological changes in MI due to the variations in the PDF characteristics of each subband signal of the 12 lead ECG signals. Due to these reasons, the aforementioned features have higher accuracy, sensitivity and specificity values for the detection of MI.

Similarly, we have evaluated the overall performance of the DNN classifier using 108 dimensional skewness, kurtosis, and entropy FVs of 12-lead ECG for the detection of MI. Table III and Table IV depict the performance of DNN classifier by considering hold-out cross-validation and 5-fold cross-validation based selection of ECG instances. The number of neurons in first and second hidden layers is used as 230 and 125, respectively. It is evident that the performance of DNN classifier with skewness features is improved by 20% with respect to the average performance of the skewness features of all ECG leads. Similarly, for entropy and kurtosis features, the performance improvement is 1% and 2% using DNN classifier. The first two layers of the proposed DNN architecture contain more neurons as compared to the number of input neurons. This helps minimize the correlation between the features by projecting to the higher dimensional hidden layer space. This may be the reason for the improvement of the performance of the DNN classifier using the skewness features of 12-lead ECG. The entropy features have higher performance in each fold as compared to other features using DNN classifier. The above observations reveal that the features extracted from the FBSE-EWT subband signals successfully capture the variations in the clinical features of 12-lead ECG for the assessment of MI pathology.

We have compared the performance of DNN classifier with various existing approaches using only 12-lead ECG signals and the comparison results are shown in Table VI. It is evident that some of the existing approaches have evaluated various morphological features from ECG signals of all leads for the detection of MI [9] [7] [46] [14]. Evaluation of such features requires the detection of the starting and end points of the clinical components of ECG such as P-wave, QRS-complex and T-wave along each lead [47] [43]. The medical practitioners manually inspect deviation in the morphology of 12-lead ECG morphological features by drawing the boundaries or the starting and end points of each clinical components [48]. This process is cumbersome and may increase the chances for the false prediction of the pathology. Other methods reported in the literature have used various feature extraction approaches over wavelet domain of 12-lead ECG signal for the detection of MI [15] [17] [6]. The predefined wavelet basis functions or filters are required for the multiscale analysis of 12-lead ECG and it is also evident that the performance of the proposed method is higher than the wavelet-based techniques for the MI detection. The advantages of the proposed work for MI detection are given as follows. The FBSE-EWT approach is utilized for the efficient time-scale decomposition of 12-lead ECG and diagnostic feature extraction. The entropy features from the subband signals of each lead ECG have higher performance with average accuracy more than 96%. The fine-tuning is not required for the proposed DNN architecture and only layer-wise pre-training is useful for getting higher accuracy value for the detection of MI. The DNN classifier such as DL-LSSVM can be used for classification of pathologies from other biomedical signals. Instead of extracting various features from the subband signals, the deep autoencoder can directly be utilized to extract the learned features from the subband signals of 12-lead ECG. Other DNN technique which is based on the sparse autoencoder and relevance vector machine can be developed for the detection of MI from the subband signals of 12-lead ECG [49]. We have also compared the performance of the proposed approach using ANN [50] and SVM [51] classifiers coupled with FBSE-EWT entropy features of 12-lead ECG. The DL-LSSVM classifier performance is higher as compared to the ANN (230 neurons in the hidden layer, average accuracy as 96.28%, average sensitivity as 95.51%, and average specificity as 97.05%), and SVM (RBF kernel, and the kernel parameter as $\sigma = 9.83$, average accuracy as 97.08%, average sensitivity as 97.96%, and average specificity as 98.65%) classifiers. The DL-LSSVM with one hidden layer has less accuracy, sensitivity, and specificity values as compared with the proposed two hidden layer DNN classifier. Due to higher performance, the proposed approach can be implemented in real-time for the automated detection of MI from ECG signals of multiple electrodes.

V. CONCLUSION

In this paper, the FBSE-EWT based time-scale analysis of 12-lead ECG has been proposed for the detection of MI pathology. The first nine subband signals have been considered based on FBSE-EWT based multiresolution analysis of 12-lead ECG. The kurtosis, the skewness and the entropy feature vectors (FVs) are evaluated from 12-lead ECG. The statistical analysis of the features demonstrates that the entropy features are more significant for the detection of MI pathology as compared to kurtosis and skewness features of 12-lead ECG. The DL-LSSVM based deep neural network has been proposed for the detection. The DNN classifier with entropy FV has higher performance as compared to both skewness and kurtosis FVs. As compared to the state-of-art features of 12-lead ECG, the proposed FBSE-EWT features have higher accuracy, sensitivity and specificity values for the detection of MI. In future, the deep learning techniques such as the deep belief network (DBN) and CNN can be used for the classification of different categories of MI using the subband signals of 12-lead ECG.

TABLE IV
PERFORMANCE OF DNN CLASSIFIERFOR 5-FOLD CROSS-VALIDATION SCHEME WITH FVS FROM 12-LEAD ECG.

Feature Vector	Measures	Fold 1	Fold 2	Fold 3	Fold 4	Fold 5	Average
Skewness FV ($\mathbf{FV}_S$)	Accuracy (%)	98.48	98.78	98.17	98.58	98.98	98.60 ± 0.30
	Sensitivity (%)	98.93	98.75	99.10	98.57	98.93	98.86 ± 0.20
	Specificity (%)	97.88	98.82	96.94	98.58	99.05	98.26 ± 0.85
Kurtosis FV ($\mathbf{FV}_K$)	Accuracy (%)	99.29	99.29	98.98	99.18	99.49	99.25 ± 0.18
	Sensitivity (%)	99.82	99.46	98.93	99.64	99.46	99.46 ± 0.33
	Specificity (%)	98.58	99.06	99.06	98.58	99.52	98.96 ± 0.39
Entropy FV ($\mathbf{FV}_E$)	Accuracy (%)	100	99.89	100	100	100	99.97 ± 0.04
	Sensitivity (%)	100	100	100	100	100	100 ± 0.00
	Specificity (%)	100	99.76	100	100	100	99.95 ± 0.10

TABLE V
COMPARISON WITH EXISTING METHODS FOR THE CLASSIFICATION OF MI AND HC USING ONLY 12-LEAD ECG.

Features Extracted	Classifier	Accuracy (%)	Sensitivity (%)	Specificity (%)	Processing (Number of Features)
ST and T-wave morphological features [9]	ANN	NA	95	86.73	Beat specific (72)
Various morphological features of 12-lead ECG [7]	KNN	NA	99.97	99.90	Beat specific (72)
Polynomial coefficents of ST-segments [14]	MIL	NA	91.43	77.29%	Beat specific (74)
Multiscale energy and eigenspace features [15]	SVM	96	93	99	Frame specific (72)
Duration features of clinical components and statistical features [46]	SVM	98.33	96.66	100	Beat specific (72)
Wavelet based features [6]	KNN	98.80	99.45	96.27	Beat specific (47)
Multiscale higher order singular value decomposition based feature extraction [17]	SVM	95.30	94.60	96.00	Beat specific (35)
FBSE-EWT features (Proposed work)	DL-LSSVM	99.74 (Hold-out)	99.87 (Hold-out)	99.60 (Hold-out)	Frame specific (108)
FBSE-EWT features (Proposed work)	DL-LSSVM	99.97 (5-Fold)	100 (5-Fold)	99.95 (5-Fold)	Frame specific (108)

REFERENCES

[1] P. T. O'gara, F. G. Kushner, D. D. Ascheim, D. E. Casey, M. K. Chung, J. A. De Lemos, S. M. Ettinger, J. C. Fang, F. M. Fesmire, B. A. Franklin *et al.*, "2013 accf/aha guideline for the management of st-elevation myocardial infarction: executive summary: a report of the american college of cardiology foundation/american heart association task force on practice guidelines," *Journal of the American College of Cardiology*, vol. 61, no. 4, pp. 485–510, 2013.

[2] S. Yusuf, S. Hawken, S. Ôunpuu, T. Dans, A. Avezum, F. Lanas, M. McQueen, A. Budaj, P. Pais, J. Varigos *et al.*, "Effect of potentially modifiable risk factors associated with myocardial infarction in 52 countries (the interheart study): case-control study," *The lancet*, vol. 364, no. 9438, pp. 937–952, 2004.

[3] H. Yang, "Multiscale recurrence quantification analysis of spatial cardiac vectorcardiogram signals," *IEEE Transactions on Biomedical Engineering*, vol. 58, no. 2, pp. 339–347, 2011.

[4] J. J. Bax, H. Baumgartner, C. Ceconi, V. Dean, R. Fagard, C. Funck-Brentano, D. Hasdai, A. Hoes, P. Kirchhof, J. Knuuti *et al.*, "Third universal definition of myocardial infarction," *Journal of the American College of Cardiology*, vol. 60, no. 16, pp. 1581–1598, 2012.

[5] S. Ansari, N. Farzaneh, M. Duda, K. Horan, H. B. Andersson, Z. D. Goldberger, B. K. Nallamothu, and K. Najarian, "A review of automated methods for detection of myocardial ischemia and infarction using electrocardiogram and electronic health records," *IEEE reviews in biomedical engineering*, vol. 10, pp. 264–298, 2017.

[6] U. R. Acharya, H. Fujita, V. K. Sudarshan, S. L. Oh, M. Adam, J. E. Koh, J. H. Tan, D. N. Ghista, R. J. Martis, C. K. Chua *et al.*, "Automated detection and localization of myocardial infarction using electrocardiogram: a comparative study of different leads," *Knowledge-Based Systems*, vol. 99, pp. 146–156, 2016.

[7] M. Arif, I. A. Malagore, and F. A. Afsar, "Detection and localization of myocardial infarction using k-nearest neighbor classifier," *Journal of medical systems*, vol. 36, no. 1, pp. 279–289, 2012.

[8] A. K. Dohare, V. Kumar, and R. Kumar, "Detection of myocardial infarction in 12 lead ecg using support vector machine," *Applied Soft Computing*, vol. 64, pp. 138–147, 2018.

[9] B. Hedén, H. Ohlin, R. Rittner, and L. Edenbrandt, "Acute myocardial infarction detected in the 12-lead ecg by artificial neural networks," *Circulation*, vol. 96, no. 6, pp. 1798–1802, 1997.

[10] H. Lu, K. Ong, and P. Chia, "An automated ecg classification system based on a neuro-fuzzy system," in *Computers in Cardiology 2000*. IEEE, 2000, pp. 387–390.

[11] P. De Chazal, M. O'Dwyer, and R. B. Reilly, "Automatic classification of heartbeats using ecg morphology and heartbeat interval features," *IEEE transactions on biomedical engineering*, vol. 51, no. 7, pp. 1196–1206, 2004.

[12] F. Badilini, M. Merri, J. Benhorin, and A. Moss, "Beat-to-beat quantification and analysis of st displacement from holter ecgs: a new approach to ischemia detection," in *Computers in Cardiology 1992, Proceedings of.* IEEE, 1992, pp. 179–182.

[13] S. Mitra, M. Mitra, and B. B. Chaudhuri, "A rough-set-based inference engine for ecg classification," *IEEE Transactions on instrumentation and measurement*, vol. 55, no. 6, pp. 2198–2206, 2006.

[14] L. Sun, Y. Lu, K. Yang, and S. Li, "Ecg analysis using multiple instance learning for myocardial infarction detection," *IEEE transactions on biomedical engineering*, vol. 59, no. 12, pp. 3348–3356, 2012.

[15] L. Sharma, R. Tripathy, and S. Dandapat, "Multiscale energy and eigenspace approach to detection and localization of myocardial infarction," *IEEE transactions on biomedical engineering*, vol. 62, no. 7, pp. 1827–1837, 2015.

[16] R. Tripathy and S. Dandapat, "Detection of cardiac abnormalities from multilead ecg using multiscale phase alternation features," *Journal of medical systems*, vol. 40, no. 6, p. 143, 2016.

[17] S. Padhy and S. Dandapat, "Third-order tensor based analysis of multilead ecg for classification of myocardial infarction," *Biomedical Signal Processing and Control*, vol. 31, pp. 71–78, 2017.

[18] M. Sharma, R. San Tan, and U. R. Acharya, "A novel automated diagnostic system for classification of myocardial infarction ecg signals using an optimal biorthogonal filter bank," *Computers in biology and medicine*, 2018.

[19] V. N. Varghees and K. Ramachandran, "Effective heart sound

segmentation and murmur classification using empirical wavelet transform and instantaneous phase for electronic stethoscope," *IEEE Sensors Journal*, vol. 17, no. 12, pp. 3861–3872, 2017.
[20] A. Bhattacharyya, L. Singh, and R. B. Pachori, "Fourier–bessel series expansion based empirical wavelet transform for analysis of non-stationary signals," *Digital Signal Processing*, vol. 78, pp. 185–196, 2018.
[21] R. Tripathy, M. R. A. Paternina, J. G. Arrieta, and P. Pattanaik, "Automated detection of atrial fibrillation ecg signals using two stage vmd and atrial fibrillation diagnosis index," *Journal of Mechanics in Medicine and Biology*, vol. 17, no. 07, p. 1740044, 2017.
[22] U. R. Acharya, H. Fujita, S. L. Oh, Y. Hagiwara, J. H. Tan, and M. Adam, "Application of deep convolutional neural network for automated detection of myocardial infarction using ecg signals," *Information Sciences*, vol. 415, pp. 190–198, 2017.
[23] S. Xu, M. Mak, and C. Cheung, "Towards end-to-end ecg classification with raw signal extraction and deep neural networks." *IEEE journal of biomedical and health informatics*, 2018.
[24] J. Xu, L. Xiang, Q. Liu, H. Gilmore, J. Wu, J. Tang, and A. Madabhushi, "Stacked sparse autoencoder (ssae) for nuclei detection on breast cancer histopathology images," *IEEE transactions on medical imaging*, vol. 35, no. 1, pp. 119–130, 2016.
[25] R. K. Tripathy, A. Z. Mendez, S. de la O, M. R. Arrieta Paternina, J. G. Arrieta, G. R. Naik *et al.*, "Detection of life threatening ventricular arrhythmia using digital taylor fourier transform," *Frontiers in Physiology*, vol. 9, p. 722, 2018.
[26] V. Bajaj and R. B. Pachori, "Classification of seizure and nonseizure eeg signals using empirical mode decomposition," *IEEE Transactions on Information Technology in Biomedicine*, vol. 16, no. 6, pp. 1135–1142, 2012.
[27] M. Oeff, H. Koch, R. Bousseljot, and D. Kreiseler, "The ptb diagnostic ecg database," *National Metrology Institute of Germany*, 2012.
[28] A. L. Goldberger, L. A. Amaral, L. Glass, J. M. Hausdorff, P. C. Ivanov, R. G. Mark, J. E. Mietus, G. B. Moody, C.-K. Peng, and H. E. Stanley, "Physiobank, physiotoolkit, and physionet: components of a new research resource for complex physiologic signals," *Circulation*, vol. 101, no. 23, pp. e215–e220, 2000.
[29] J. Gilles, "Empirical wavelet transform," *IEEE Transactions on Signal Processing*, vol. 61, no. 16, pp. 3999–4010, 2013.
[30] R. B. Pachori and P. Sircar, "Analysis of multicomponent am-fm signals using fb-desa method," *Digital Signal Processing*, vol. 20, no. 1, pp. 42–62, 2010.
[31] ——, "A new technique to reduce cross terms in the wigner distribution," *Digital Signal Processing*, vol. 17, no. 2, pp. 466–474, 2007.
[32] J. Schroeder, "Signal processing via Fourier-Bessel series expansion," *Digital Signal Processing*, vol. 3, no. 2, pp. 112–124, 1993.
[33] R. B. Pachori and P. Sircar, "EEG signal analysis using FB expansion and second-order linear TVAR process," *Signal Processing*, vol. 88, no. 2, pp. 415–420, 2008.
[34] P. Jain and R. B. Pachori, "Event-based method for instantaneous fundamental frequency estimation from voiced speech based on eigenvalue decomposition of the Hankel matrix," *IEEE/ACM Transactions on Audio, Speech and Language Processing (TASLP)*, vol. 22, no. 10, pp. 1467–1482, 2014.
[35] R. B. Pachori and P. Sircar, "Non-stationary signal analysis: Methods based on Fourier-Bessel representation," *LAP LAMBERT Academic Publishing, Germany*, 2010.
[36] J. Gilles and K. Heal, "A parameterless scale-space approach to find meaningful modes in histogramsApplication to image and spectrum segmentation," *International Journal of Wavelets, Multiresolution and Information Processing*, vol. 12, no. 06, p. 1450044, 2014.
[37] I. Daubechies, *Ten lectures on wavelets, CBMS-NSF Regional Conference Series in Applied Mathematics, SIAM, Philadelphia, PA, USA*, 1992, vol. 61.
[38] C. Therrien and M. Tummala, *Probability and random processes for electrical and computer engineers*. CRC press, 2011.
[39] R. Tripathy and S. Dandapat, "Detection of myocardial infarction from vectorcardiogram using relevance vector machine," *Signal, Image and Video Processing*, vol. 11, no. 6, pp. 1139–1146, 2017.
[40] E. Jayachandran *et al.*, "Analysis of myocardial infarction using discrete wavelet transform," *Journal of medical systems*, vol. 34, no. 6, pp. 985–992, 2010.
[41] A. Ng, "Sparse autoencoder," *CS294A Lecture Notes, p. 72*, 2011.
[42] J. A. Suykens, T. Van Gestel, and J. De Brabanter, *Least squares support vector machines*. World Scientific, 2002.
[43] L. G. Tereshchenko and M. E. Josephson, "Frequency content and characteristics of ventricular conduction," *Journal of electrocardiology*, vol. 48, no. 6, pp. 933–937, 2015.
[44] A. L. Goldberger, Z. D. Goldberger, and A. Shvilkin, *Clinical Electrocardiography: A Simplified Approach E-Book*. Elsevier Health Sciences, 2017.
[45] G. D. Ruxton, "The unequal variance t-test is an underused alternative to student's t-test and the mann–whitney u test," *Behavioral Ecology*, vol. 17, no. 4, pp. 688–690, 2006.
[46] B. Liu, J. Liu, G. Wang, K. Huang, F. Li, Y. Zheng, Y. Luo, and F. Zhou, "A novel electrocardiogram parameterization algorithm and its application in myocardial infarction detection," *Computers in biology and medicine*, vol. 61, pp. 178–184, 2015.
[47] Y. Zigel, A. Cohen, and A. Katz, "The weighted diagnostic distortion (wdd) measure for ecg signal compression," *IEEE Transactions on Biomedical Engineering*, vol. 47, no. 11, pp. 1422–1430, 2000.
[48] B. Surawicz and T. Knilans, *Chou's Electrocardiography in Clinical Practice E-Book: Adult and Pediatric*. Elsevier Health Sciences, 2008.
[49] H. Tripathy, D. Bej, P. Pattanaik, D. Mishra, S. Kamilla, and R. Tripathy, "Measurement of zone temperature profile of a resistive heating furnace through rvm model," *IEEE Sensors Journal*, vol. 18, no. 11, pp. 4429–4435, 2018.
[50] S. S. Haykin *et al.*, *Neural networks and learning machines/Simon Haykin*. New York: Prentice Hall,, 2009.
[51] C. Cortes and V. Vapnik, "Support-vector networks," *Machine learning*, vol. 20, no. 3, pp. 273–297, 1995.

Rajesh Kumar Tripathy received the B.Tech degree in Electronics and Telecommunication Engineering from the Biju Patnaik University of Technology (BPUT), Odisha, India, in 2009, and the M.Tech degree in Biomedical Engineering from the National Institute of Technology (NIT) Rourkela, Rourkela, India, in 2013, and the PhD degree in Electronics and Electrical Engineering (EEE) from the Indian Institute of Technology (IIT) Guwahati, Guwahati, India in 2017. Currently, he is working as an Assistant Professor in the department of Electrical and Electronics Engineering (EEE), Birla Institute of Technology and Science (BITS), Pilani, Hyderabad Campus. His research interests are Biomedical Signal Processing, Sensor Data Processing, Machine Learning and Medical Image Processing. He has published research papers in reputed international journals and conferences.

Abhijit Bhattacharyya received the B.E. (Hons.) degree from the University of Burdwan, Burdwan, India, and the M.Tech. degree from National Institute of Technology (NIT) Jalandhar, Jalandhar, India, both in Electronics and Communication engineering, in 2010 and 2013, respectively. He has received the Ph.D. degree in Electrical Engineering at Indian Institute of Technology Indore, Indore, India in 2018. During PhD, he was awarded Raman-Charpak fellowship 2017 by Indo-French Centre for the Promotion of Advanced Research (IFCPAR). Under this fellowship, he worked at the Research Center for Automatics, Nancy, France/ CRAN UMR 7039 University of Lorraine CNRS. Currently, he is a faculty member with the Department of Electronics and Communication Engineering, NIT Andhra Pradesh, Tadepalligudem, India. He has published nine papers in International journals and conferences. His research interests include biomedical signal processing (with an emphasis to EEG signals), non-stationary signal processing, spatial filtering, source separation, and machine learning.

Ram Bilas Pachori received the B.E. degree with honours in Electronics and Communication Engineering from Rajiv Gandhi Technological University, Bhopal, India in 2001, the M.Tech. and Ph.D. degrees in Electrical Engineering from Indian Institute of Technology (IIT) Kanpur, Kanpur, India in 2003 and 2008, respectively. He worked as a Postdoctoral Fellow at Charles Delaunay Institute, University of Technology of Troyes, Troyes, France during 2007-2008. He served as an Assistant Professor at Communication Research Center, International Institute of Information Technology, Hyderabad, India during 2008-2009. He served as an Assistant Professor at Discipline of Electrical Engineering, IIT Indore, Indore, India during 2009-2013. He worked as an Associate Professor at Discipline of Electrical Engineering, IIT Indore, Indore, India during 2013-2017 where presently he has been working as a Professor since 2017. He is also an Associated Faculty with Discipline of Biosciences & Biomedical Engineering at IIT Indore. He is also a Visiting Professor at School of Medicine, Faculty of Health and Medical Sciences, TaylorŁs University, Subang Jaya, Malaysia since December 2018. He worked as a Visiting Scholar at Intelligent Systems Research Center, Ulster University, Northern Ireland, UK during December 2014. He is an Associate Editor of Biomedical Signal Processing and Control journal and an Editor of IETE Technical Review journal. He is a senior member of IEEE and a Fellow of IETE. He has more than 150 publications which include journal papers, conference papers, books, and book chapters. His publications have around 3500 citations, h index of 32, and i10 index of 70 (Google Scholar, January 2019). He has served on review boards for more than 85 scientific journals and served for scientific committees of various national and international conferences. His research interests are in the areas of biomedical signal processing, non-stationary signal processing, speech signal processing, signal processing for communications, computer-aided medical diagnosis, and signal processing for mechanical systems.